Nanowire Quantum Dots as an Ideal Source of Entangled Photon Pairs

Ranber Singh and Gabriel Bester
Max Planck Institute for Solid State Research, D-70569 Stuttgart, Germany
(Received 10 March 2009; published 3 August 2009)

We predict that heterostructure quantum wires and [111] grown quantum dots have a vanishing fine-structure splitting on the grounds of their symmetry, and are therefore ideal candidates to generate entangled photon pairs. We underpin this proposal by atomistic million-atom many-body pseudopotential calculations of realistic structures and find that the vanishing fine-structure splitting is robust against possible variations in morphology.

DOI: 10.1103/PhysRevLett.103.063601 PACS numbers: 73.21.Hb, 42.50.−p, 73.21.La, 78.67.Hc

At the heart of the emerging fields of quantum teleportation [1], quantum cryptography [2], and quantum information [3] is the generation and the manipulation of entangled quantum states. These intriguing states are the key to the utilization of the recently engineered manifold of nanostructures. A popular proposal [4] involves the use of semiconductor quantum dots as a source of entangled photons. In this scheme, polarization-entangled photons can be produced by the cascade emission process, biexciton ($|XX\rangle$) $\rightarrow$ exciton($|X\rangle$) $\rightarrow$ ground state($|0\rangle$) [4], where the polarization of the photon pair is determined by the spin of the intermediate exciton state. In an idealized QD with degenerate intermediate exciton states the polarization of the first photon (stemming from $|XX\rangle \rightarrow |X\rangle$) is entangled with the second photon (stemming from $|X\rangle \rightarrow |0\rangle$) [4]. Entanglement requires the so-called ''which path information'' to be lost. This proposal, therefore, relies on a vanishing excitonic fine structure [5] which is *a priori* not given. Indeed, the electron and hole are subject to exchange interactions which usually lead to splittings of the exciton energy [7,8]. A tremendous ongoing effort to *tune* this fine-structure splitting (FSS) includes the use of electric fields [9], strain [10], magnetic fields [11], and local annealing techniques [12]. Other approaches include spectral filtering [6] or the selection of QDs with low FSSs [13]. Indeed, most of the epitaxial semiconductor quantum dots (QDs) are grown along the [001] direction and exhibit FSSs as a consequence of the atomistic symmetry of the structures, spin-orbit interaction and the electron-hole exchange interaction [14]. It is possible to separate these three effects and formally derive the origin of the FSS [14]. Here, we use a different approach where we develop an understanding for FSSs using arguments based on the interface symmetry to finally numerically calculate their values for realistic structures. We predict that [111] nanowire QDs have vanishing FSSs on grounds of their symmetry, bypassing the need for experimentally demanding setups [6,9–13], and constitute ideal candidates for the generation of entangled photon pairs.

The T_d [15] point group symmetry of III-V zinc blende semiconductors is reduced to D_{2d} in an ideal symmetric quantum well grown in the crystallographic direction [001]. However, the microscopic symmetry of each interface in the quantum well is lower [16], namely C_{2v}, lacking the rotoinversion operation (S_4) existing in D_{2d}. Hence, the presence of two ideal and compensating interfaces is required in order to ''restore'' the higher D_{2d} symmetry of the global structure and obtain a vanishing FSS. In order for FSS to appear, the symmetry must be lower than D_{2d}, as in a structure with asymmetric interfaces. An electric field [17] in growth direction (point group $C_{\infty v}$), for instance, breaks the symmetry of both interfaces, lowering the global symmetry to C_{2v} (Pockels effect [17]) and introduces FSSs. Intrinsically, a heterostructure without a common atom, e.g., InAs/GaP (as opposed to a common atom heterostructure such as InAs/GaAs) has inequivalent interfaces, hence (depending on the number of ML in the superlattice) C_{2v} symmetry [18] and exhibits FSS. Alternatively, the interfaces can have defects, such as monolayer steps, and localise either the hole or the electron, or both [16,19], leading to C_{2v} or lower symmetry and FSS. The emergence of fine structure in self-assembled QDs can be naturally understood from this point of view: The dots are usually grown on top of a narrow quantum well (wetting layer). Their base represents an ideal interface. Their top, however, is curved (e.g., lens shaped) very much *unlike* the bottom interface. In the extreme case of a pyramidal QD, one can show that the four facets of the dot, forming the ''top'' interface form compensating pairs which are globally isotropic [20], so that there is no counterpart to the bottom interface. The deviation from D_{2d} symmetry is therefore extreme and the FSS consequently large.

While this is reasonably well understood, we now turn our attention to heterostructure quantum wires composed of a sequence of different semiconductors [see inset in Fig. 1(d)], potentially forming a quantum well within the wire, enabling a three dimensional confinement of carriers, forming another type of QD. A wide range of different material combinations have been recently synthesized including [111]-oriented InAsP/InP semiconductor nanowire QDs with cylindrical shape [21,22], InP nanowires grown on GaP (111)B substrates with zinc blende structure [23], GaAs nanowires grown on [111]-oriented substrates

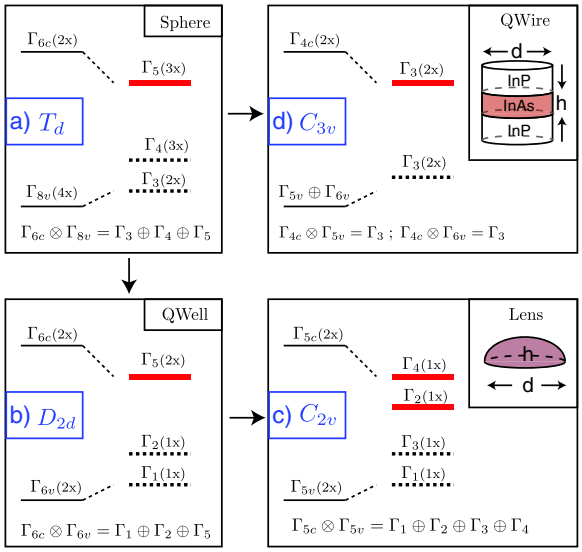

FIG. 1 (color online). Symmetry analysis of different nanostructures. The left column of each panel gives the symmetry of the valence band maximum and the conduction band minimum. The right column gives the resulting excitons with their corresponding point group symmetries. A thick red (black dashed) line indicates optically bright (dark) states.

with mainly wurtzite structure [24], recently, Shtrikman *et al.* grew purely zinc blende GaAs nanowires [25] and Samuelson *et al.* synthesized zinc blende [001]-oriented InP and InAs/InP nanowires [26].

Before we performed numerical calculations of the FSS in these structures, we analyzed the excitonic symmetry using group theory [15] arguments. In Fig. 1 we show four cases corresponding to different structures and their respective symmetry. Figure 1(a) gives the results for T_d symmetry which corresponds to bulk, or to a spherical dot, with zinc blende structure. The left column gives the symmetry of the conduction band minimum (CBM) as Γ_{6c} and the valence band maximum (VBM) as Γ_{8v} with a degeneracy of four ($4x$), including spin. These are the well-known degenerate (at Brillouin zone center) heavy- and light-hole bands. The right column gives the excitonic symmetry obtained as the direct product of CBM and VBM. A red line stands for optically bright states and a dashed black line for dark states. The bright states are threefold degenerate and there is no fine structure. In Fig. 1(b) we reduce the symmetry to D_{2d}, as given in quantum wells grown along [001]. Still the bright states are degenerate without FSS. If we further reduce the symmetry to C_{2v} [Fig. 1(c)], as given in [001] grown self-assembled QDs, the two bright states correspond to different point group representations and can split. This is the group theoretical result we described earlier using qualitative arguments involving the interfaces. Another route to symmetry lowering is to start from T_d [Fig. 1(a)] and consider structures grown along the [111] direction leading to the C_{3v} point group [Fig. 1(d)]. This is also the point group of QDs with wurtzite structure. Thus, the point group symmetry of [111]-oriented nanowire QDs is C_{3v}, whether it is pure wurtzite or zinc blende or has both coexisting phases [27]. The key result of this investigation is that in a quantum wire grown along the [111] direction, or in a QD grown on (111) substrate, both having C_{3v} symmetry, the bright states correspond to the same, degenerate representation (Γ_3), *forbidding* a FSS. This would remain true for wurtzite heterostructure wires and for QDs in the form of disks grown along [001] (D_{2d} symmetry). In order for this central result to be relevant to *realistic* structures, as opposed to the idealized symmetry arguments, we performed numerical calculations of the FSS. We chose a set of several different nanostructures summarized in Table I. Some shapes, composition and sizes are directly taken from recent experiments [21,22]. Shapes $S1$, $S2$, and $S3$ are, three [111]-oriented nanowire QDs embedded in InP. $S1$ and $S2$ are made of InAs with circular and hexagonal cross sections, respectively, and $S3$ is circular and made of $InAs_{0.25}P_{0.75}$. Likewise, $S8$, $S12$, and $S13$ are typical self-assembled QDs. Some other shapes are used to demonstrate our symmetry-based arguments in the following.

The calculations are performed using the empirical pseudopotential approach and configuration interaction [28–30]. The calculation of fine-structure splitting is demanding because of the atomistic origin of FSS [14] and the large structures involved. The structures considered here require the calculation of the many-body wave functions of around 3.0×10^6 atoms.

In the top of Fig. 2 we show the square of the wave functions (probability density) for the first three electron ($e_{0,1,2}$) and hole ($h_{0,1,2}$) states for the InAs/InP structures $S1$, $S5$, $S7$, $S8$ and $S9$ (Table I). For the shapes $S1$ and $S5$

TABLE I. Exciton transition energies ($|X\rangle$ PL) and FSSs of InAsP/InP and InGaAs/GaAs nanostructures. Shape $S2$ is a hexagonal prism. The sizes are given as diameter [d] and height [h] and in terms of elongation for $S9$.

	QD material	Shape	Size (d,h) (nm)	$\|X\rangle$ PL (eV)	FSS (μeV)
		InAsP/InP			
$S1$	InAs [111]	disk (C_{3v})	33.0, 8.0	0.817	0.2
$S2$	InAs [111]	hex (C_{3v})	35.0, 8.0	0.823	0.0
$S3$	$InAs_{0.25}P_{0.75}$ [111]	disk (C_{3v})	33.0, 8.0	1.331	0.0
$S4$	InAs [111]	disk (C_{3v})	25.2, 3.5	0.965	0.1
$S5$	InAs [111]	lens (C_{3v})	25.2, 3.5	1.020	0.1
$S6$	InAs [001]	disk (D_{2d})	33.0, 8.0	0.705	0.0
$S7$	InAs [001]	disk (D_{2d})	25.2, 3.5	0.801	0.0
$S8$	InAs [001]	lens (C_{2v})	25.2, 3.5	0.836	12.9
		elong.	5%, 3.5	0.965	2.8
$S9$	InAs [111]	disk (C_S)	10%, 3.5	0.965	5.4
			15%, 3.5	0.965	8.2
		InGaAs/GaAs			
$S10$	InAs [001]	disk (D_{2d})	33.0, 8.0	0.911	0.0
$S11$	InAs [001]	disk (D_{2d})	25.2, 3.5	0.945	0.0
$S12$	InAs [001]	lens (C_{2v})	25.2, 3.5	1.010	2.6
$S13$	$In_{0.6}Ga_{0.4}As$ [001]	lens (C_{2v})	25.2, 3.5	1.256	5.8

with circular base grown along [111] we can recognize the threefold symmetry (especially in states h_2) of the C_{3v} point group. For the self-assembled QDs grown along [001] ($S8$) the electron P states (e_1, e_2), are orientated along the $[1\bar{1}0]$ and [110] directions and are energetically split by 2 meV, a typical signature of the C_{2v} symmetry. The lens shape dots grown along [111] ($S5$) has only one fully confined electron state in contrast to the one grown along [001] with same dimensions ($S8$). This difference is due to the larger hydrostatic strain inside the dot grown along [111], compared to the [001] grown structure. Also for the $InAs_{0.25}P_{0.75}/InP$ quantum wire dot ($S3$) only one electron (not shown) is confined due to, in this case, the low As concentration and shallow confinement. The corresponding absorption spectra are given in the lower part of Fig. 2. The lines form three groups that can be attributed to interband S-S, P-P, and D-D transitions. Since the states are not pure angular momentum states, some additional cross transitions appear. The FSSs of the lowest energy transitions (marked with an X in Fig. 2) are given in Table I. For all the structures with D_{2d} and C_{3v} symmetry we obtain, within our numerical accuracy of about 0.2 μeV, a vanishing FSS. An important result is that this remains valid for the alloyed wire QD (S3) made of $InAs_{0.25}P_{0.75}$. This structure was simulated by placing the arsenic and phosphorous anions randomly on their lattice sites, as given in a random alloy, keeping the overall arsenic composition at 25%. This process destroys, strictly speaking, the atomistic symmetry. However, our calculations show that, the FSS is not significantly affected by the randomness of the structure and the FSS still vanishes. Another important observation is that an InAs lens shape dot grown along the [111] direction has vanishing FSS. This was predicted by symmetry arguments and is confirmed here. Unlike the case of [001] grown structures, where the equivalence of the interfaces (as argued above) is the key to a vanishing FSS, in the [111] structures (e.g., $S5$), no such equivalence is required. Indeed, the upper and lower interfaces of structure $S5$ are very different and the FSS still vanishes. Note that the piezoelectric fields do not lower the symmetry. We included piezoelectric effects up to second order in the calculations of $S2$ and find a lowering of the exciton transition from 0.823 eV to 0.816 eV but 0.0 μeV FSS [31]. In contrast, in the extensively studied [001] grown structures [7,8,14], such as $S8$, $S12$, $S13$, the inequivalent interfaces leads to significant FSSs.

Now that we have established that structures grown along the [111] direction have a vanishing FSSs if they are circular or hexagonal in the (111) plane (as a disk, lens, or hexagonal prism), we deform them to assess how robust the results are against possible other malformations of the structure. Inequivalent interfaces do not lead to lower symmetry, but an elongation of the quantum wire's cross section brings the symmetry down, from C_{3v} to C_s, and the twofold degenerate bright excitons may split, akin to the case of structures with C_{2v} symmetry [Fig. 1(c)]. To quantitatively appreciate this effect, we have simulated wires with an elliptical cross section (indexed as $S9$; see Table I) with major axis d_1 along the $[1\bar{1}0]$ direction and minor axis d_2 along the $[11\bar{2}]$ direction. In Fig. 2 we see that the probability density of the first electron (e_1) and first hole P levels (h_1) follow the global shape's major axis along the $[1\bar{1}0]$ direction. The C_{3v} symmetry, obvious in the case of the circular disk, $S1$, is now replaced by the lower C_s symmetry with only one reflection plane and the states look qualitatively similar to the C_{2v} lens, $S8$. The three groups of lines in absorption spectrum are now broadened due to the splitting of the P and D states, widening the range of possible P-P and D-D transitions. The FSS indicated in Fig. 2 for $S9$ is plotted in Fig. 3(b)] as a function of the elongation, d_1/d_2, (keeping $d_1 d_2 = 25.2^2$ nm^2). The dependence of the FSS on the elongation is nearly linear with a FSS of 3 μeV for an elongation of 5%. Experimentally there is no evidence of any elongation in

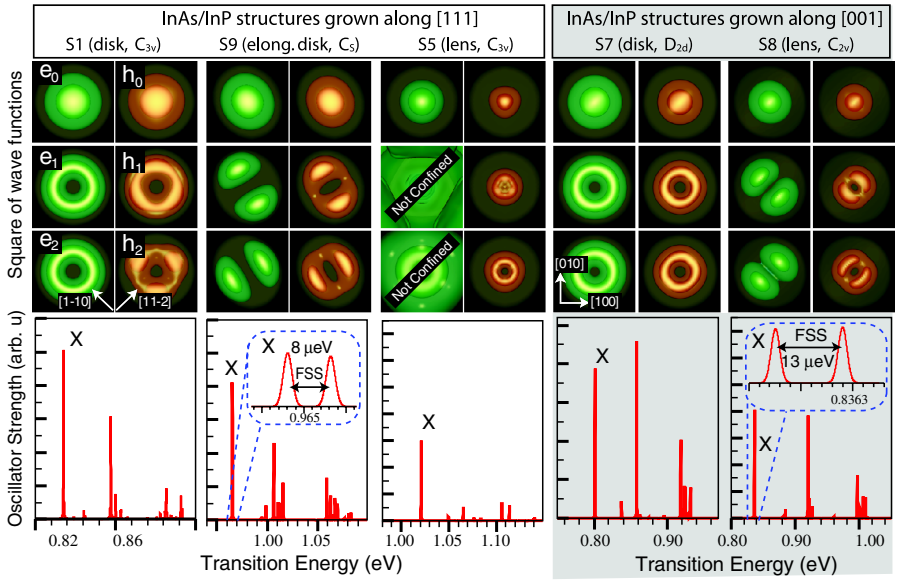

FIG. 2 (color online). Square of the wave functions for the first three electron (e_0, e_1, e_2) and hole (h_0, h_1, h_2) states of the structures $S1$, $S5$, $S7$, $S8$, and $S9$, described in Table I. The isosurfaces enclose 75% of the probability densities. Corresponding absorption spectra in arbitrary units. The inset for structure $S9$ and $S10$ is a blowup of the excitonic line separated by the FSS (lower part).

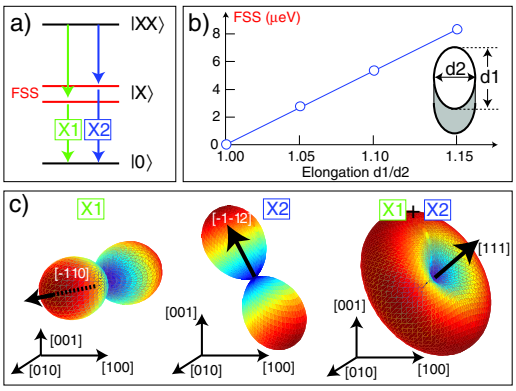

FIG. 3 (color online). (a) Schematic of the biexciton cascade with FSS and transitions $X1$ and $X2$. (b) FSS as a function of elongation for the shape $S9$ of Table I. (c) Polar plots of the oscillator strength of the transitions $X1$, $X2$ and the sum of both. The polar axis represents the E-field direction of light.

the cross section of the wires [21,22,25–27,32,33]. Our numerical calculations show that even if the wire's cross section is not perfectly round or hexagonal, no sudden increase of FSS should be expected. Also a micro faceting of the hexagonal wire as described in [34] should not lead to increased fine structure (see [31]).

In the case of nonvanishing FSS [schematically shown in Fig. 3(a)], the two bright states, $X1$ and $X2$, emit polarized light. In Fig. 3(c) we plot the oscillator strength of the transitions as a polar plot where the polar axis gives the direction of the light's electric field vector. The lower energy transition is polarized mostly along the $[1\bar{1}0]$ direction (i.e., along the major axis) and the higher energy transition along the $[11\bar{2}]$ direction. The sum of these transitions reconstructs an optical signal which has a small in-plane anisotropy of 1.2%, 2.2%, and 3.2% for the elongations 5%, 10%, and 15%, respectively. However, one must be careful with the linear relationship between in-plane anisotropy and elongation. Our alloyed dot $S3$ has a perfectly circular cross section but a polarization anisotropy of 2%, comparable to the pure InAs structure $S9$ with 10% elongation. So that the atomic fluctuation of concentration leads to significant anisotropy but not to FSS. Recent measurements of the polarization anisotropy [22] suggest that wires can have very low in-plane anisotropies. Experimentally, FSSs have not been observed in heterostructure nanowires until today, which is in agreement with our predictions. However, only few optical experiments [22] were performed on single wires with a resolution high enough to detect FSSs. There is no fundamental limitation for such measurements to be performed in the near future.

We show that based on symmetry arguments, quantum nanostructures grown along the [111] direction, such as self-assembled quantum dots or heterostructure quantum wires must have a vanishing FSS. We confirm this prediction by million-atom empirical pseudopotential many-body calculations of *realistic* InAsP/InP and InGaAs/GaAs structures. We use experimentally realized shapes, compositions and sizes and find that the vanishing FSS must be present in experimentally realized structures. We further study how robust the results are against deformations and conclude that [111] grown structures, especially heterostructure wires, are ideal candidates for the generation of entangled photon pairs. Through the control of size, shape and composition they would emit at the optical fiber communication wavelength (conventional C band) of 1.55 μm (0.8 eV). The suggested structures, and their atomistic symmetry, are tolerant of imperfections in their interfaces, unlike [001] grown structures, which should boost their attractiveness.

[1] T. Jennewein *et al.*, Phys. Rev. Lett. **88**, 017903 (2001).
[2] N. Gisin *et al.*, Rev. Mod. Phys. **74**, 145 (2002).
[3] J. Chen *et al.*, Phys. Rev. Lett. **100**, 133603 (2008).
[4] O. Benson *et al.*, Phys. Rev. Lett. **84**, 2513 (2000).
[5] For a significant degreee of entanglement the fine-structure splitting should be below the excitonic linewidth of typically 1 μeV [6].
[6] N. Akopian *et al.*, Phys. Rev. Lett. **96**, 130501 (2006).
[7] M. Bayer *et al.*, Phys. Rev. Lett. **82**, 1748 (1999).
[8] R. J. Warburton *et al.*, Nature (London) **405**, 926 (2000).
[9] K. Kowalik *et al.*, Appl. Phys. Lett. **86**, 041907 (2005).
[10] S. Seidl *et al.*, Appl. Phys. Lett. **88**, 203113 (2006).
[11] R. Stevenson *et al.*, Nature (London) **439**, 179 (2006).
[12] W. Langbein *et al.*, Phys. Rev. B **69**, 161301(R) (2004).
[13] R. Hafenbrak *et al.*, New J. Phys. **9**, 315 (2007).
[14] G. Bester, S. Nair, and A. Zunger, Phys. Rev. B **67**, 161306 (R) (2003).
[15] G. F. Koster, J. O. Dimmock, R. G. Wheeler, and H. Satz, *Properties of the Thirty-Two Point Groups* (MIT Press, Cambridge, MA, 1963).
[16] H. W. van Kesteren, E. C. Cosman, W. A. J. A. van der Poel, and C. T. Foxon, Phys. Rev. B **41**, 5283 (1990).
[17] S. H. Kwok *et al.*, Phys. Rev. Lett. **69**, 973 (1992).
[18] O. Krebs and P. Voisin, Phys. Rev. Lett. **77**, 1829 (1996).
[19] D. Gammon *et al.*, Phys. Rev. Lett. **76**, 3005 (1996).
[20] G. Bester and A. Zunger, Phys. Rev. B **71**, 045318 (2005).
[21] E. Minot *et al.*, Nano Lett. **7**, 367 (2007).
[22] M. H. M. van Weert *et al.*, arXiv:0808.2908 (2008).
[23] Y. Watanabe *et al.*, Thin Solid Films **464–465**, 248 (2004).
[24] M. Tchernycheva *et al.*, Nanotechnology **17**, 4025 (2006).
[25] H. Shtrikman *et al.*, Nano Lett. **9**, 215 (2009).
[26] U. Krishnamachari, Appl. Phys. Lett. **85**, 2077 (2004).
[27] K. Tomioka *et al.*, Jpn. J. Appl. Phys. **46**, L1102 (2007).
[28] L.-W. Wang and A. Zunger, Phys. Rev. B **59**, 15 806 (1999).
[29] A. Franceschetti, H. Fu, L.-W. Wang, and A. Zunger, Phys. Rev. B **60**, 1819 (1999).
[30] G. Bester, J. Phys. Condens. Matter **21**, 023202 (2009).
[31] See EPAPS Document No. E-PRLTAO-103-022934 for supplementary information containing four figures and text on two pages. For more information on EPAPS, see http://www.aip.org/pubservs/epaps.html.
[32] C. Thelander *et al.*, Mater. Today **9**, 28 (2006).
[33] W. Lu and C. M. Lieber, J. Phys. D **39**, R387 (2006).
[34] J. Johansson *et al.*, Nature Mater. **5**, 574 (2006).